water

Article

Study of Snap Loads for Idealized Mooring Configurations with a Buoy, Inextensible and Elastic Cable Combinations for the Multi-Float M4 Wave Energy Converter

Peter Stansby [1,*] and Efrain Carpintero Moreno [1,2]

1 School of Engineering, University of Manchester, Manchester M13 9PL, UK; efrain.carpinteromoreno@ugent.be
2 Department of Civil Engineering, Ghent University, 9000 Ghent, Belgium
* Correspondence: p.k.stansby@manchester.ac.uk

Received: 22 August 2020; Accepted: 7 October 2020; Published: 11 October 2020

Abstract: There has been considerable modelling and wave basin validation of the multi-mode, multi-float, moored wave energy converter M4. The 6 float (2 power take off) (PTO) configuration is considered here with mooring from a buoy with light inextensible cables. Large mean mooring forces and very large peak or snap forces were measured in large waves while the rotational response about the hinges (for power take off in operational conditions) was predominantly linear. Modelling has been extended with elastic mooring cables connected directly to the base of the bow float and to the buoy. The experimental mean force is input to the linear diffraction/radiation model. The device response is effectively unchanged. The peak mooring force and tensions remain large with direct connection to the base of the bow float but are only slightly greater than the mean forces with elastic cables to the buoy, and an elastic hawser provides a further slight reduction. For the largest waves measured, the force was about 10% of the dry weight of the platform. The idealized efficient modelling may inform more detailed design while efficient methods for determining highly nonlinear mean forces remain to be established.

Keywords: wave energy converter; multi-float; mooring configurations; elastic cables; mooring buoy; snap loads

1. Introduction

Many concepts for offshore wave energy conversion have been considered and devices are generally classed as point absorbers, terminators or attenuators, e.g., see reviews [1,2]. Moorings are a generic problem for survivability and fatigue life. The basic hinged raft-type attenuator concept has been developed into multi-float form with multi-mode forcing and multiple power take offs to give capacities similar to offshore wind turbines, a system known as M4 which is considered here [3,4]. There has been considerable modelling and wave tank validation of M4 [3–6], demonstrating relatively high capture widths, up to about one wavelength corresponding to the energy period in irregular waves or three stern float diameters, for the 6 float version. This is shown in a video frame from laboratory testing in Figure 1, the scale being approximately 1:50. This version has one bow float, three mid floats and two stern floats, called 1-3-2; the stern floats are connected by beams to hinges above the outer mid floats for power take off (PTO), provided by mechanical damping from an actuator. The mooring connection is made to the bow float. The system heads naturally into the wave direction due to wave drift forces. The experiments were undertaken with a simple single point mooring (SPM), with the buoy connected by a light inextensible cable (hawser) to a point just above the deck of the bow float. The buoy was connected to the bed also by a light inextensible cable, primarily for station keeping but mooring force was also measured. JONSWAP wave spectra were used. Linear diffraction-radiation modelling gave good predictions of rotational response for operational conditions (with significant wave height H_s about 4 cm or 2 m full scale) and also surprisingly for large waves with the PTO disengaged in survival mode [6]. Response was also shown to be predominantly linear in direct analysis of experimental data for the 3-float (1-1-1) configuration in large focused waves [7]. However mean loads increased markedly with significant wave height H_s and snap loads were considerably larger than the mean. The modelling indicated that the mooring had negligible effect on response and power capture in operational conditions, as the mooring may easily be switched off in the model. In the experiments, connecting the hawser to a buoy or an overhead gantry also made negligible difference [6]. We are concerned here with mooring systems which reduce snap loads.

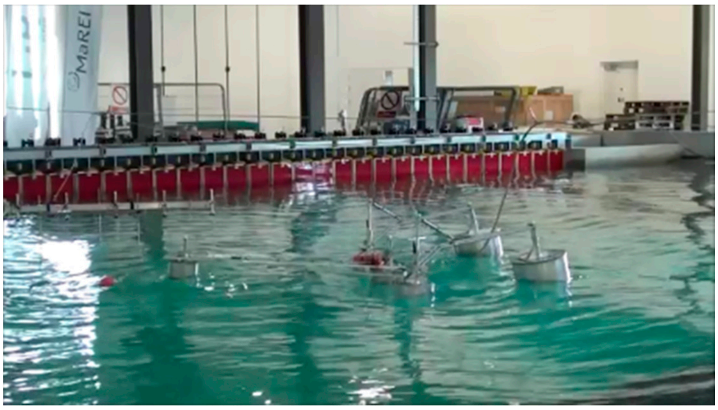

Figure 1. A video frame of the 6-float M4 with single mooring buoy (red, partly submerged) in the Lir ocean basin, University College Cork.

We need to consider the origin of the mean loads. In diffraction/radiation analysis to 2nd order, mean drift forces are due to: zero-difference frequencies in a wave spectrum, as on a fixed body, generally defined by quadratic transfer functions obtained by potential flow panel methods such as WAMIT [8]; radiation damping as wave energy flux is converted into body motion (for all degrees of freedom); drag damping as wave energy flux is converted into viscous losses (negligible for the case considered here). This requires an estimate of wave speed to convert total energy flux into force, assumed equal to total flux divided by spectral energy in [6]. In the case of wave energy converters, wave energy flux is also absorbed in mechanical damping. This formulation gave only approximate mean force prediction for operational conditions and was grossly underestimated in large waves [6]. There are highly nonlinear effects in large waves, e.g., increasing asymmetry (about a crest) as breaking is approached in extreme conditions. This will give a non-zero Froude Krylov (FK) force (due the undisturbed pressure field). In linear diffraction/radiation analyses the oscillatory FK force is included in the diffraction or excitation force (e.g., in WAMIT) with another component due to wave scattering. That the response is predominantly linear suggests that radiation damping produced by body motion will also be linear. The nonlinear mean force is difficult to predict and here the measured experimental mean forces are applied as an external force in linear diffraction/radiation analysis [6]. Since oscillatory response is reasonably well predicted, we assume that oscillating loads are predicted correspondingly and may be superimposed on the mean forces. The dynamic mooring loads may be compared with experimental measurements using inextensible cables and the aim is to determine how different mooring configurations with elastic cables may reduce snap loads.

There are various design guidelines for moorings in conventional ocean engineering applications, for oil/gas and wind platforms, often of catenary form, e.g., [9]. While withstanding peak loads is essential, inhibiting and damping platform motion by mooring is an added benefit. However, wave energy conversion requires platform motion and damping is detrimental [10–13]. There is a widespread consensus in the wave energy community that mooring system design and modelling is a major challenge that needs to be overcome [12].

Various mooring configurations have been proposed for wave energy converters (WECs) including catenary, SPM, taut elastic and combinations including clump masses and risers (or jumpers), e.g., [13–17]. Coupled mooring and hydrodynamic modelling studies have been undertaken usually for point absorbers with computational fluid dynamics (CFD), e.g., [18,19] and reviewed in [11]. Linear models have also been extended to account for nonlinear FK and drag effects, e.g., [20,21].

The aim here is to investigate, by linear diffraction/radiation modelling with empirical mean forces, how the dynamic mooring loads for the 6-float attenuator-type WEC M4 may be reduced by replacing the inextensible cables to the buoy with taut elastic cables, attached directly to the bow float, to the buoy with inextensible hawser, and to the buoy with an elastic hawser. The paper is structured as follows. The mooring models linked to the existing hydrodynamic model are described in Section 2. Results are presented in Section 3 and discussed in Section 4. Some conclusions are drawn in Section 5.

2. Model

The M4 device was tested experimentally in the ocean wave basin at Lir, Cork [5,6], and a video frame is shown in Figure 1. The red mooring buoy is visible and there are light inextensible cords attaching the buoy to the bed and the buoy to the device. The scale is about 1:50 and the elevation dimensions are shown in Figure 2 and the plan dimensions in Figure 3. The bow float is denoted 1, the three mid floats 2, 3, 4 and the stern floats 5, 6.

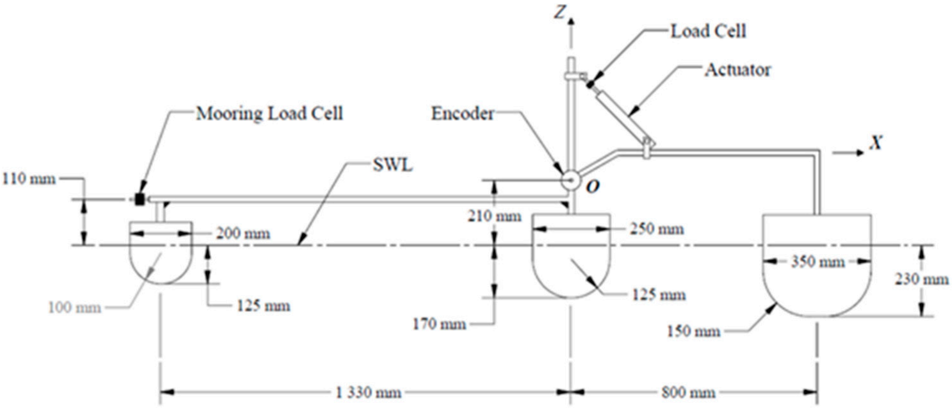

Figure 2. Elevation dimensions of physical model.

The hydrodynamic model with mooring is the same as in [6]. In summary, multi-body equations are set up with reference to the hinge point O in Figure 2, above the central mid float. Hydrodynamic forcing due to surge, heave, sway, pitch and roll is input. With uni-directional waves yaw is negligible. Body motion about the longitudinal centerline would not occur due to symmetry. Although the damping in the power take off (PTO) on either side was not generally equal, sway and roll were negligible. With irregular waves, Cummins' formulation was applied with hydrodynamic coefficients from WAMIT [8]. In addition, a mean hydrodynamic force is applied which is balanced by the mean mooring force. Here we input the measured mean force which is independent of mooring configuration, provided that this does not affect device response. There is negligible drag in operational conditions and for large response agreement with experiment is improved with a small drag coefficient; 0.2 is applied. This is consistent with some idealized CFD simulations [22]. The equation set is solved for position of O, x_O, y_O, z_O, (with y_O effectively zero), the angular rotation of the bow-mid (effectively rigid) frame (including floats 1,2,3,4) about O, θ_{1234}, and the angular rotation of stern floats 5 and 6 about O, θ_5, θ_6. Equations are solved to give accelerations at each time step and velocities and displacements are advanced. The mooring provides a quasi-static external force, described below. With PTO engaged, the pneumatic actuators generate a torque at each hinge due to the relative angular velocity between frame 1234 and beams to floats 5 and 6: $\dot{\theta}_{r5} = \dot{\theta}_{1234} - \dot{\theta}_5$ and $\dot{\theta}_{r6} = \dot{\theta}_{1234} - \dot{\theta}_6$. With linear damping: $Q_5 = B_5\dot{\theta}_{r5}$, $Q_6 = B_6\dot{\theta}_{r6}$, where constants B_5, B_6 are determined by post processing the measurements and were found to be almost constant but not equal (differing by up to 30%), despite using identical parts. The difference between θ_5 and θ_6 was however very small [5] and mean $\dot{\theta}_r = (\dot{\theta}_{r5} + \dot{\theta}_{r6})/2$ is presented here. Mechanical power is given by torque x relative angular velocity and found to be only weakly sensitive to coefficient B. Without the PTO engaged for large wave heights, θ_5 and θ_6 were almost identical.

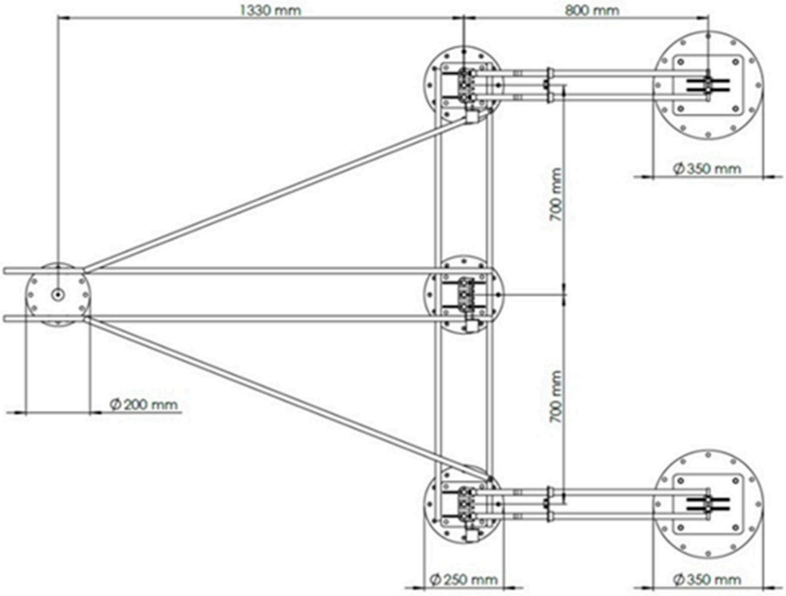

Figure 3. Plan dimensions of physical model.

Three mooring configurations are considered:

A. the experimental configuration with light inextensible cords (Dyneema) attaching a buoy to the bed and the buoy to the device. The cord in water is assumed to be neutrally buoyant.
B. elastic cords attached to the base of the bow float, with elastic stiffness based on Froude scaling.
C. same elastic cords attached to the buoy in A with an inextensible cord from buoy to the bow float.
D. same elastic cords as C but with cord to bow float (hawser) also elastic.

2.1. Configuration A

The experimental configuration is shown in Figure 4.

The mooring force is assumed to be quasi-static with negligible inertia in the cables with the only force on the buoy due to buoyancy and its weight. The water surface is simply assumed to be horizontal within linearized approximation.

The mooring lines are shown in Figure 4 with the small spherical buoy of 0.11 m diameter and mass 87 g. The aim is to determine the horizontal and vertical restraining mooring forces at the fairlead F, H_M, V_M. The buoy weight is W and buoyancy force B, due to submergence d. The submerged depth d in still water is 0.024 m, shown in Figure 5. When the lines are taut the forces at the fairlead F are shown in Figure 5 with T for tension force such that

$$H_M = T_2 cos(\beta_2), \tag{1}$$

$$V_M = T_2 sin(\beta_2) \tag{2}$$

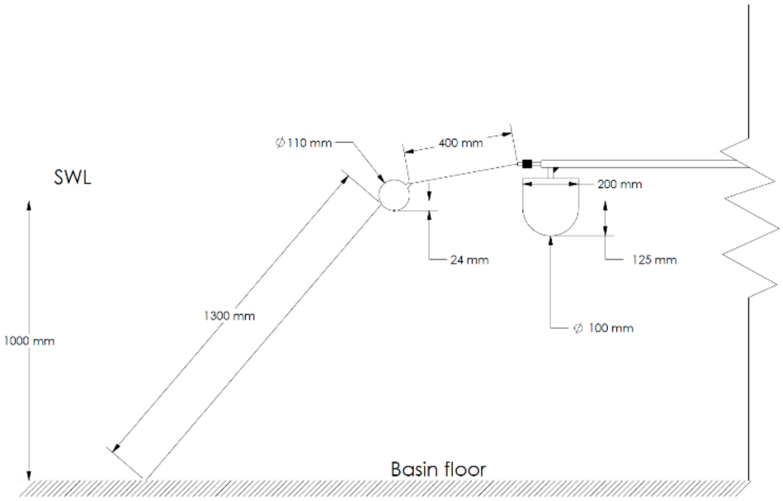

Figure 4. Dimensions of experimental configuration with inextensible cables connected to the buoy.

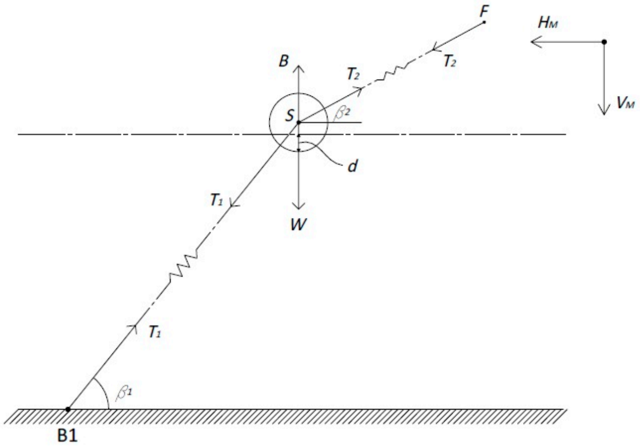

Figure 5. Notation for configuration A.

F is defined by the motion of the hinge point O and the rotation about the hinge point. Thus, the displacement from the initial position is

$$x'_F = x_O - v_F sin(\theta_{1234}) \tag{3}$$

$$z'_F = z_O + h_F\ sin(\theta_{1234}) \tag{4}$$

where h_F is the horizontal distance from O to F, v_F is vertical distance of F below O. At each time step the new position of *F* defines the mooring force, due to the extensions in the cables.

At the buoy in the horizontal direction

$$T_2 cos(\beta_2) = T_1 cos(\beta_1) = H_M \tag{5}$$

And in the vertical

$$B - W = T_1 sin(\beta_1) - T_2 sin(\beta_2) = H_M\ (\tan(\beta_1) - \tan(\beta_2)\ ) \tag{6}$$

giving

$$H_M = \frac{(B - W)}{(\tan(\beta_1) - \tan(\beta_2))} \tag{7}$$

and hence V_M. The position of the fairlead on bow float 1 is known at each time level. We now define position of mooring connection relative to bed connection point as $x_{1b},\ z_{1b}$ and when tension is just zero as $x_{1b0},\ z_{1b0}$. If length of lines (to sphere centre) are l_1 and l_2 then

$$l_1 cos(\beta_1) + l_2 cos(\beta_2) = x_{b1} \tag{8}$$

$$l_1 sin(\beta_1) + l_2 sin(\beta_2) = z_{b1} \tag{9}$$

$\beta_1,\ \beta_2$ may thus be determined which defines submergence d and hence B and H_M and V_M. The line is slack if $x_{1b} < x_{1b0}$ and $H_M = V_M = 0$. The submergence d is determined by the vertical position of the buoy relative to the bed $l_1 sin(\beta_1)$ and $\Delta d = l_1(sin(\beta_{10}) - sin(\beta_1))$.

$$\text{For } d < 2r \quad B = \rho\, g\, \pi \frac{d^2(3r-d)}{3} \tag{10}$$

and when fully submerged

$$d > 2r \quad B = 4\,\rho\, g\, \pi \frac{r^3}{3} \tag{11}$$

2.2. Configuration B

There are two elastic mooring lines with fairlead connection F at the base of bow float as shown in Figure 6. The fore mooring line bed connection B_1 is at $x_{B1},\ z_{B1}$ and the aft B_2 is at $x_{B2},\ z_{B2}$; the fairlead point F is $x_F,\ z_F$. F is defined by the motion of the hinge point O and the rotation about the hinge point as for configuration A. At each time step, the new position of F defines the mooring force, due to the extensions in the cables. For the fore cable the length is

$$l_1 = \sqrt{((x_F + x'_F - x_{B1})^2 + (z_F + z'_F - z_{B1})^2)} \tag{12}$$

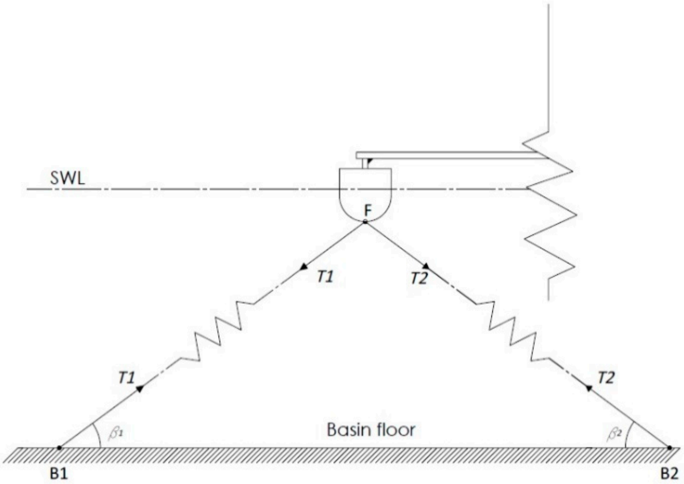

Figure 6. Notation for configuration B.

With $l_1 > l_0$, $T_1 = k\,(l_1 - l_0)$ and with $l_1 < l_0$ $T_1 = 0$ where l_0 is initial length and k is the elastic stiffness. The angle of the cable to the bed is

$$\beta_1 = tan^{-1}(\,(z_F + z'_F - z_{B1})/(x_F + x'_F - x_{B1})) \tag{13}$$

Similarly, for the aft cable

$$l_2 = \sqrt{((x_F + x'_F - x_{B2})^2 + (z_F + z'_F - z_{B2})^2)} \tag{14}$$

With $l_2 > l_0$, $T_2 = k\ (l_2 - l_0)$ and with $l_2 < l_0$ $T_2 = 0$. The angle to the bed is

$$\beta_2 = tan^{-1}\Big(\big(z_F + z'_F - z_{B2}\big)/\big(x_F + x'_F - x_{B2}\big)\Big). \tag{15}$$

The horizontal and vertical mooring forces are given by

$$H_M = T_1 cos(\beta_1) +\ T_2 cos(\beta_2) \tag{16}$$

$$V_M = T_1 \sin(\beta_1) +\ T_2 sin(\beta_2) \tag{17}$$

acting upwave and downwards at F respectively.

2.3. *Configuration C*

This configuration is similar to A with addition of cable 3 and cables 1 and 3 are elastic. The fairlead position F determines the mooring force. We know length SF is constant (inextensible) equal to 0.4 m (if not slack) but position S is not known while on the arc of a circle centre F. The lengths $SB_1 = l_1$ and $SB_3 = l_3$ determine tensions $T_1 = k\ (l_1 - l_{10})$ and $T_3 = k\ (l_3 - l_{30})$, with $l_{10},\ l_{30}$ lengths when just taut.

For horizontal equilibrium

$$T_2 = (T_1 cos(\beta_1) - T_3 cos(\beta_3))/cos(\beta_2) \tag{18}$$

Vertical equilibrium will not in general be satisfied giving error

$$dV = B - W + T_2 sin(\beta_2) - T_1 sin(\beta_1) - T_3 sin(\beta_3) \tag{19}$$

Then β_2 is varied between −30° and +90° at 1° intervals until dV changes sign and β_2 for $dV = 0$ is determined by linear interpolation. The fairlead forces are thus given by

$$H_M =\ T_2 cos(\beta_2) \tag{20}$$

$$V_M =\ T_2 sin(\beta_2) \tag{21}$$

2.4. *Configuration D*

The configuration is as Figure 7 now with cable to float SF elastic with same stiffness k. Firstly, an estimate of the length l_2 is assumed to be the slack length l_{2O} and T_2 and β_2 are evaluated as before. An elastic tension T_{2e} is given by $T_{2e} =\ k\,(l_2 - l_{2O})$. A revised length is given by $l_2\ = l_{2O} + (T_2 + T_{2e})/2k$ and T_2 and β_2 are recalculated and the iteration continues until $T_2 = T_{2e}$, single precision accuracy taking less than 10 iterations.

2.5. *Elastic stiffness*

The elastic stiffness $k =\ EA/l_0$ where E is Young's modulus, A is cross sectional area of the cable and l_0 cis the slack (just taut) length. Magnitudes of 100 and 200 N/m were applied for the results shown. This corresponds to $EA \approx 180$ and 360 N. For a scale of 1:50 this elastic stiffness corresponds to 250 and 500 kN/m at full scale (based on Froude scaling) which are practical values according to [13]. No material or hydrodynamic damping from cables is assumed in the model.

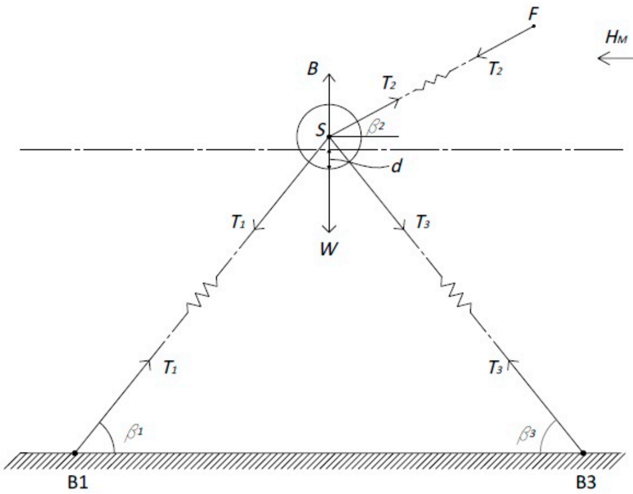

Figure 7. Notation for configuration C.

3. Results

JONSWAP wave spectra were used with a peak enhancement factor γ = 3.3. The target H_s of 0.04 and 0.06 m for operational conditions were not exactly reproduced and measured values are given the Table 1. Although the resulting spectra were close to the specified form, the measured spectra were used as input for model comparison.

Table 1. Experimental values of H_s for JONSWAP spectra with γ = 3.3.

T_p (s)	0.8	0.9	1.0	1.1	1.2	1.4	1.6	1.8	2.0
$H_s \approx 0.04$ (m)	0.035	0.037	0.038	0.038	0.039	0.038	0.037	0.038	0.041
$H_s \approx 0.06$ (m)	0.049	0.054	0.057	0.057	0.059	0.057	0.056	0.057	0.062

The experimental results (configuration A) for relative angle θ_r are shown in Figure 8 for rms and in Figure 9 for peak values with $H_s \approx 0.04$m and 0.06 m with results from the linear diffraction/radiation model with mean measured force input. The agreement is reasonably close, although note there is a maximum value of about 15 degrees ue to the actuator stroke limit which is reached for $H_s \approx 0.06$ m.

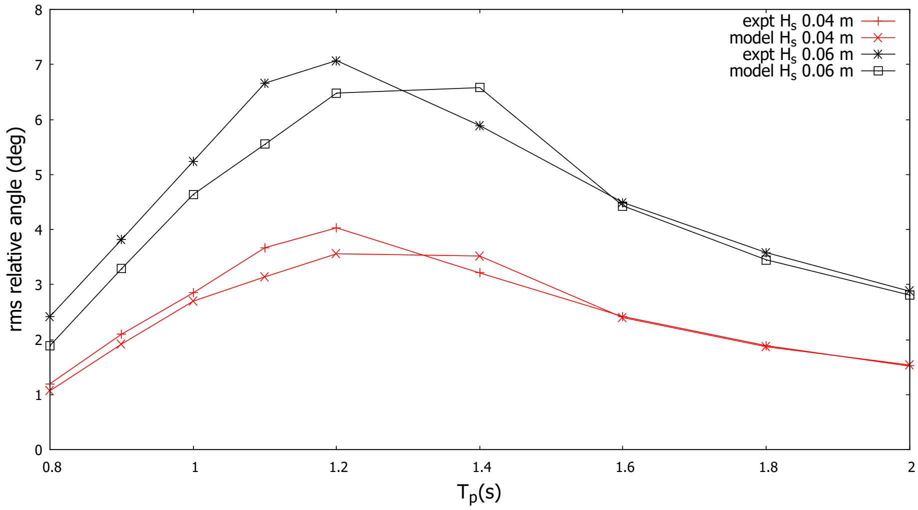

Figure 8. Variation of rms relative angle θ_r with T_p for H_s $\approx$ 0.04 m and 0.06 m from experiment and linear diffraction/radiation model with measured mean force.

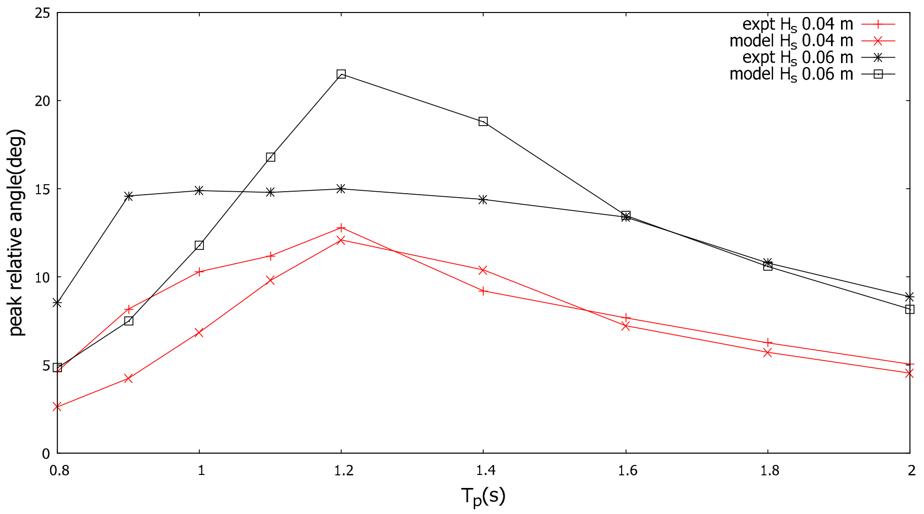

Figure 9. Variation of peak relative angle θ_r with T_p for $H_s \approx 0.04$ m and 0.06 m from experiment and linear diffraction/radiation model with measured mean force.

The power output in terms of non-dimensional capture width ratio (CWR) is shown in Figure 10. The capture width ratio, CWR, is defined as average power (P_{av})/wave power per meter crest/2x diameter of a stern float. The device width is often used to normalize capture width and, since the two stern floats drive the PTOs, the device width is set to 2× float diameter. The experimental CWR was similar for $H_s \approx 0.04$ and 0.06 m. However, the model underestimates power by up to 30% and the reasons for this are presently unexplained. Control of the PTO torque may also be employed to optimize power capture, increasing power capture by 20–40% in operational wave conditions [23].

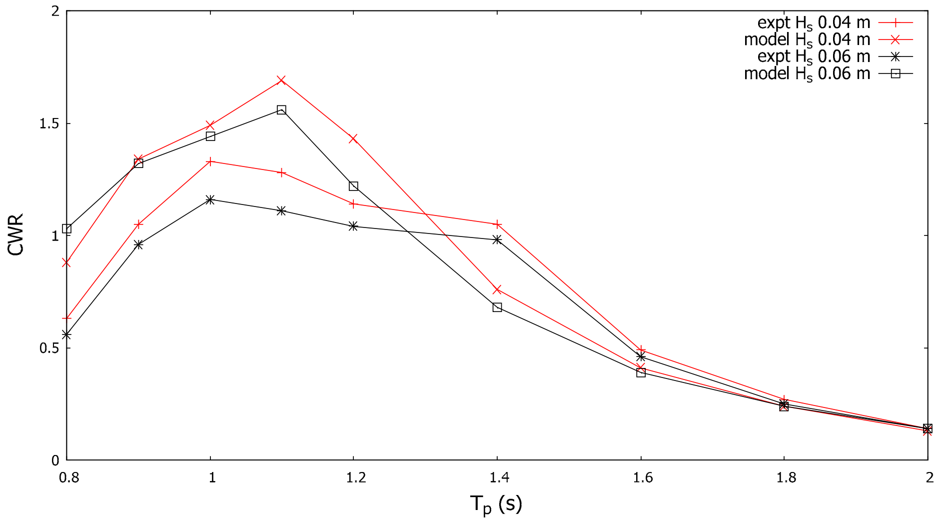

Figure 10. Variation of capture width ratio (CWR) with T_p for $H_s \approx 0.04$ m and 0.06 m from experiment and linear diffraction/radiation model with measured mean force.

This demonstrates that the body response, and hence dynamic forcing, were approximately predicted by linear modelling. We are particularly concerned with mooring loads in large waves and for these cases the actuator was disengaged so there was no mechanical damping and no end stop.

Results for rms θ_r and max θ_r are shown in Figure 11 for T_p = 1, 1.4, 2 s. The tests were of 5 min duration. The motion increased and predictions were improved with a small drag coefficient of 0.2 (for all modes). Remarkably the response was still quite well predicted except for T_p = 1s where the model underestimated.

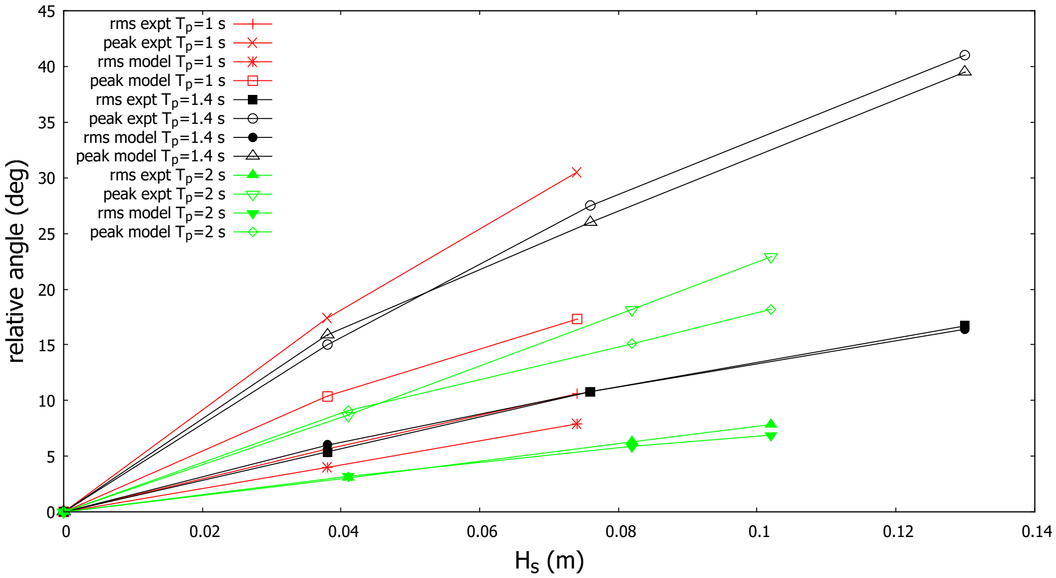

Figure 11. Variation of rms and peak relative angle θ_r with H_s for T_p = 1, 1.4, 2 s from experiment and linear diffraction/radiation model with measured mean force.

The peak horizontal force at the fairlead is shown for H_s ≈ 0.04 m and 0.06 m in Figure 12. The mean measured input into the model is also shown. The model results are generally similar although it underestimates markedly around T_p = 1 s for H_s ≈ 0.04 m and 1.1s for H_s ≈ 0.06 m, to be discussed later.

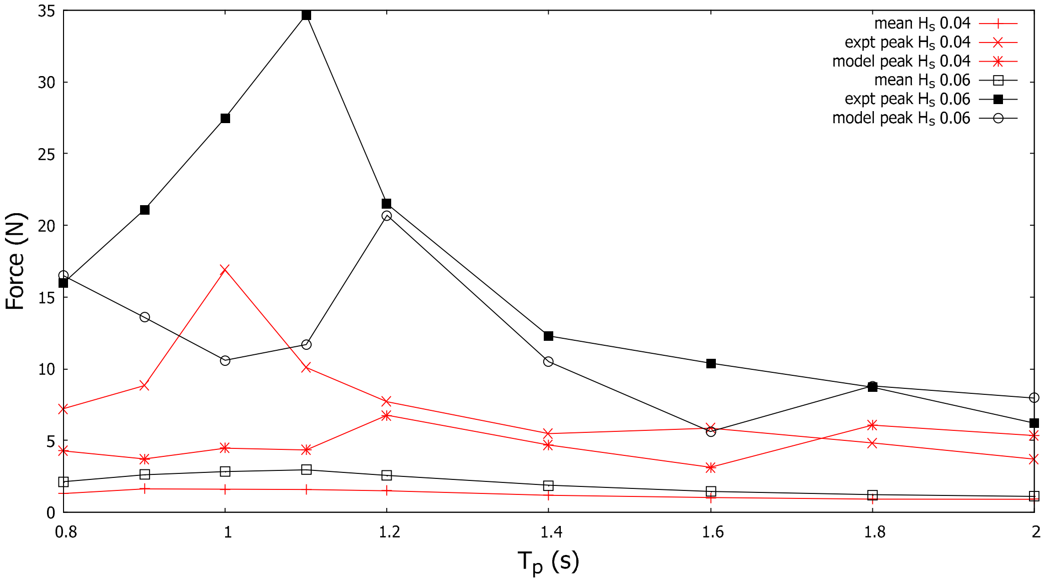

Figure 12. Variation of horizontal fairlead mooring force with T_p for H_s ≈ 0.04 m and 0.06 m from experiment and linear diffraction/radiation model with measured mean force.

Figure 13 shows the mean peak values for experimental cases with T_p = 1, 1.4, 2 s with varying H_s. The mean values clearly increased markedly for H_s > 0.04 m. The large experimental peak with H_s ≈ 0.04 m and T_p = 1 s was again apparent. The model results were quite similar for T_p = 1.4 s but may under- or overestimate the peaks, for T_p =1 s and 2 s respectively. The magnitudes can be substantial, over 100 N. The model did not include any damping due to the buoy or cables as this is difficult to quantify but artificially introducing damping in the model reduced peak values.

Although the only force on the buoy was due to buoyancy, the model picked up gross effects of peak mooring force qualitatively and the influence of elasticity will now be investigated.

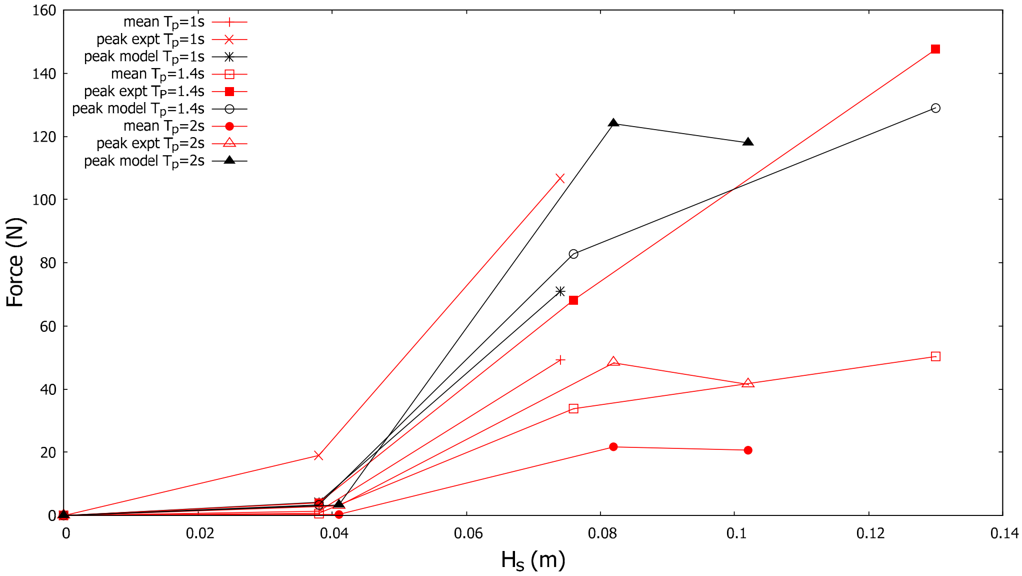

Figure 13. Variation of horizontal fairlead mooring force with H_s for T_p = 1, 1.4, 2 s from experiment and linear diffraction/radiation model with measured mean force.

For cases with direct elastic connection to the bow float (configuration B), elastic to buoy connection (configuration C) and elastic connections to buoy and bow float (configuration D), the mean and peak tensions are shown in Figure 14 for $H_s \approx 0.04$ m and Figure 15 for $H_s \approx 0.06$ m; the experimental values (configuration A) are included. The bed connections in all cases were 3 m apart and cables connecting to the bed were of equal slack (unextended) length. Note tension was slightly different from mooring force. The large experimental tensions around T_p = 1 s for $H_s \approx 0.04$ m and T_p =1.1 s for $H_s \approx 0.06$ m are discussed later but otherwise the experimental and model tensions showed similar trends. For the model results, the case with direct elastic to buoy and float (D) generally had the smallest peaks except around T_p =1 s for $H_s \approx 0.04$ m and T_p = 1.1 s for $H_s \approx 0.06$ m when the inextensible cables to buoy and float showed smaller values; this will again be discussed later. The largest overall snap tensions occured with the direct elastic connection to float (B) around T_p =1.2 s.

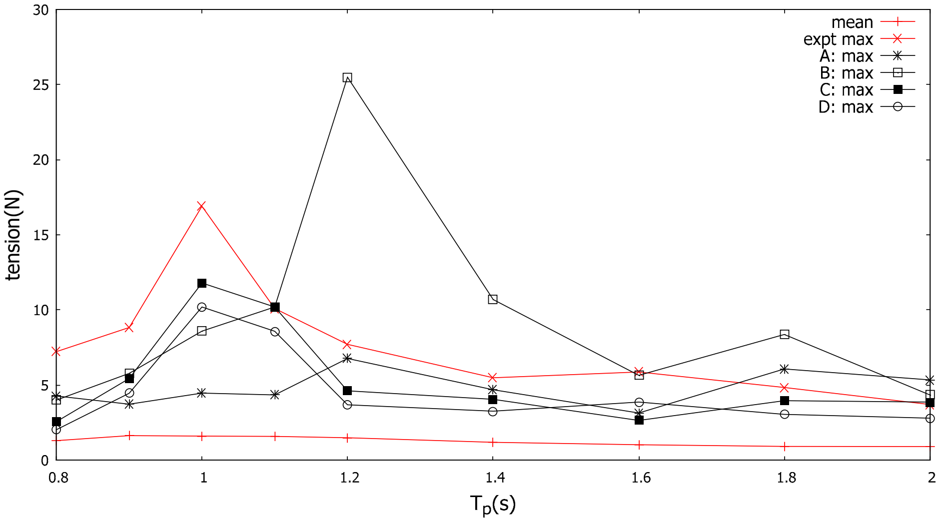

Figure 14. Variation of peak/maximum tension with T_p for $H_s \approx 0.04$ m from linear diffraction/radiation model with measured mean force and experiment.

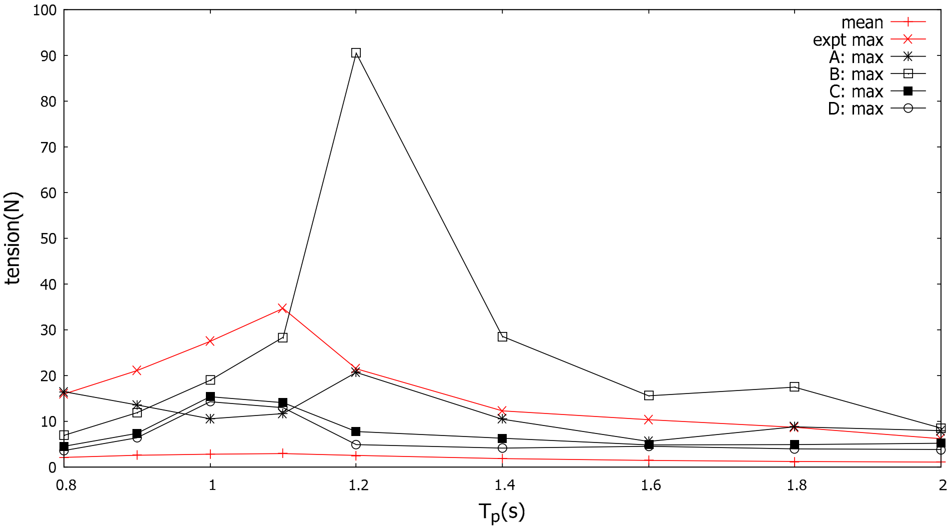

Figure 15. Variation of peak/maximum tension with T_p for $H_s \approx 0.06$ m from linear diffraction/radiation model with measured mean force and experiment.

Tensions with larger waves and disengaged PTO are shown in Figure 16 modelled for the four mooring configurations. It is clear that the large snap forces are avoided with the elastic to buoy (C) and the elastic to buoy and float configuration (D), which has slightly smaller values. The peak magnitudes were only slightly greater than the means. The direct elastic to float configuration (B) can have similar, larger or smaller magnitudes than the inextensible to buoy and float configuration (A).

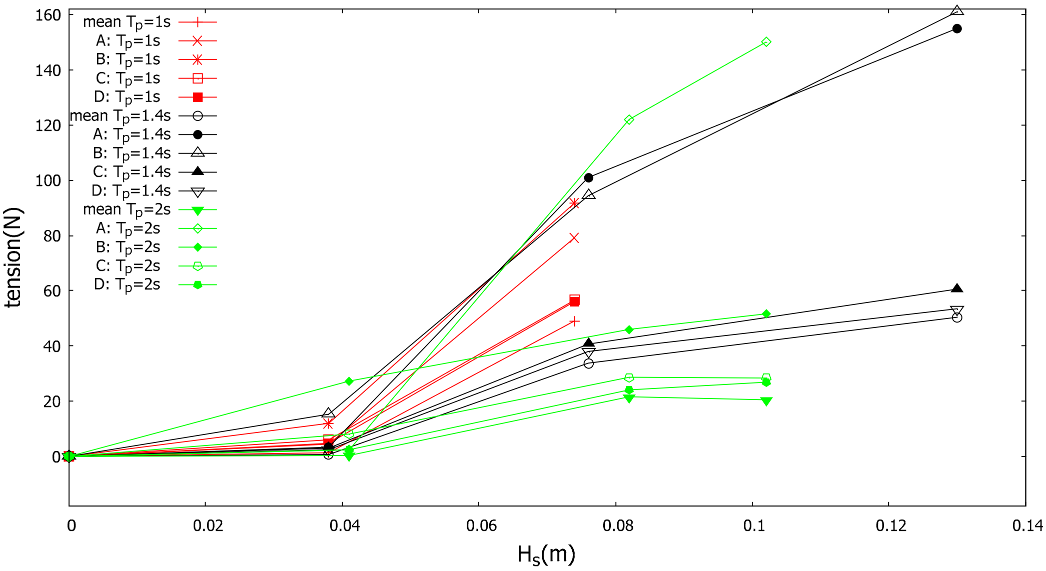

Figure 16. Variation of peak tension with H_s for T_p = 1, 1.4, 2 s from linear diffraction/radiation model with measured mean force.

4. Discussion

It has been demonstrated that elastic cables to a buoy reduce snap forces in extreme waves such that the peak force magnitude is only slightly greater than the mean forces. The mean mooring force balances the mean hydrodynamic force which is independent of mooring configuration for the same platform response. An elastic cable from buoy to float provides a further slight reduction in snap forces which is beneficial. On the other hand, elastic cables connected directly to the base of the bow float produce quite large snap forces, as large as with inextensible cables attached to the buoy in some cases. To understand this, we consider the longitudinal stiffness of the total platform. Figure 17 shows the static horizontal force variation with displacement for the four mooring configurations. The elastic stiffness of a cable was 100 N/m in all cases shown. With the inextensible cables to the buoy (configuration A) the buoy submergence acts as a form of elasticity with small stiffness for small displacement becoming large as the cables approach maximum length (become more collinear). With the elastic cable to float base (configuration B) and elastic to buoy (configuration C) the overall stiffness is almost the same, but the snap forces are much greater for B. The difference is the connection point to the float which is thus important and peak forces can be magnified due to platform motion. With elastic cables to the buoy, an elastic cable from buoy to float in addition (configuration D) causes the overall stiffness to be approximately halved as would be expected with two springs in series.

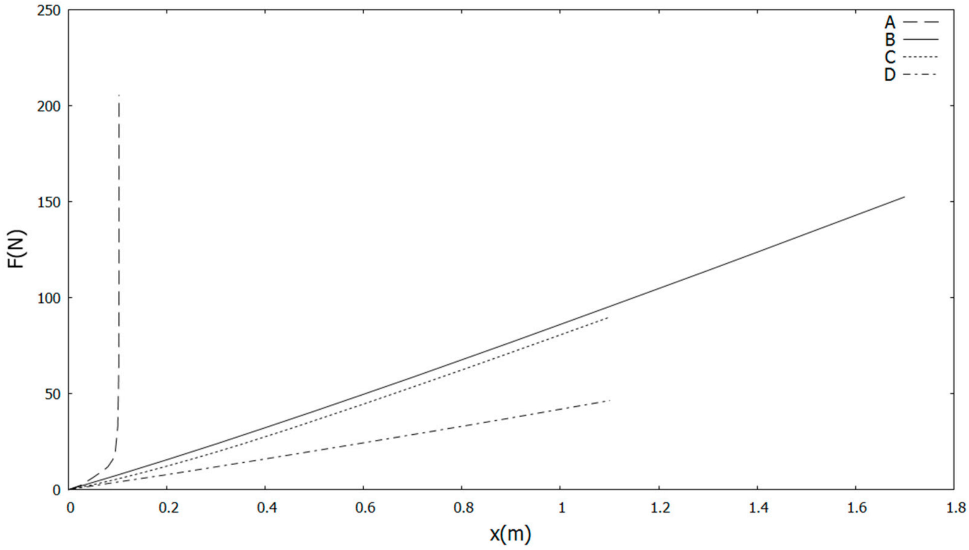

Figure 17. Variation of static mooring force F with displacement x for the four mooring configurations A, B, C, D with cable elastic stiffness of 100 N/m.

There is a relatively large peak measured mooring force around T_p = 1 s for $H_s \approx 0.04$ m and T_p = 1.1 s for $H_s \approx 0.06$ m. The experimental tension time series with T_p = 1 s for $H_s \approx 0.04$ m is shown in Figure 18a and the model time series in Figure 18b. Notably, the wavemakers start at time zero and the time scale shown starts at 50 s after transients have died away.

The natural period of the total platform in surge is relevant. The total dry mass is 55.7 kg and surge added mass is 34.0 kg giving an equivalent mass of 89.7 kg. With an equivalent stiffness k ~80 N/m the natural frequency is approximately 0.19 Hz with a period of 7 s. This period is apparent in Figure 18a,b. The big difference is the large experimental peak in Figure 18a which occurs at an interval of 128 s which is the repeat time for wave generation. This is not present in the model time series which is otherwise quite similar with high frequencies of 1 s period superimposed on the 7 s period oscillation. The float natural frequencies in heave are about 1 Hz. This large peak ceases for $T_p > 1.2$ s. Inspection of the wave elevation time series for T_p = 1 s shows that a large snap load coincides with a group of relatively large waves; the largest load occurs with a group of 5 waves with height about 5 cm. This causes the local mean load to be about $3\frac{1}{2}$ times greater than the overall mean and the snap loads are correspondingly larger than the model results (with overall mean imposed). With elastic cables to buoy and float in Figure 18c, the time series is quite different with regular force peaks when the cables are taut and zero tension when slack. The platform moves upwave from its taut condition to its slack condition due to the cable spring, then the motion is opposed by the mean force returning the platform to its taut condition. This determines the period of oscillation which appears quite constant at 19 s in this case. The peak force with elastic cables is still quite low at less than 10 N, but greater than the model results with inextensible cables with overall mean imposed but less than the experimental results with wave group effects. There are corresponding effects for $H_s \approx 0.06$ m and T_p = 1.1 s.

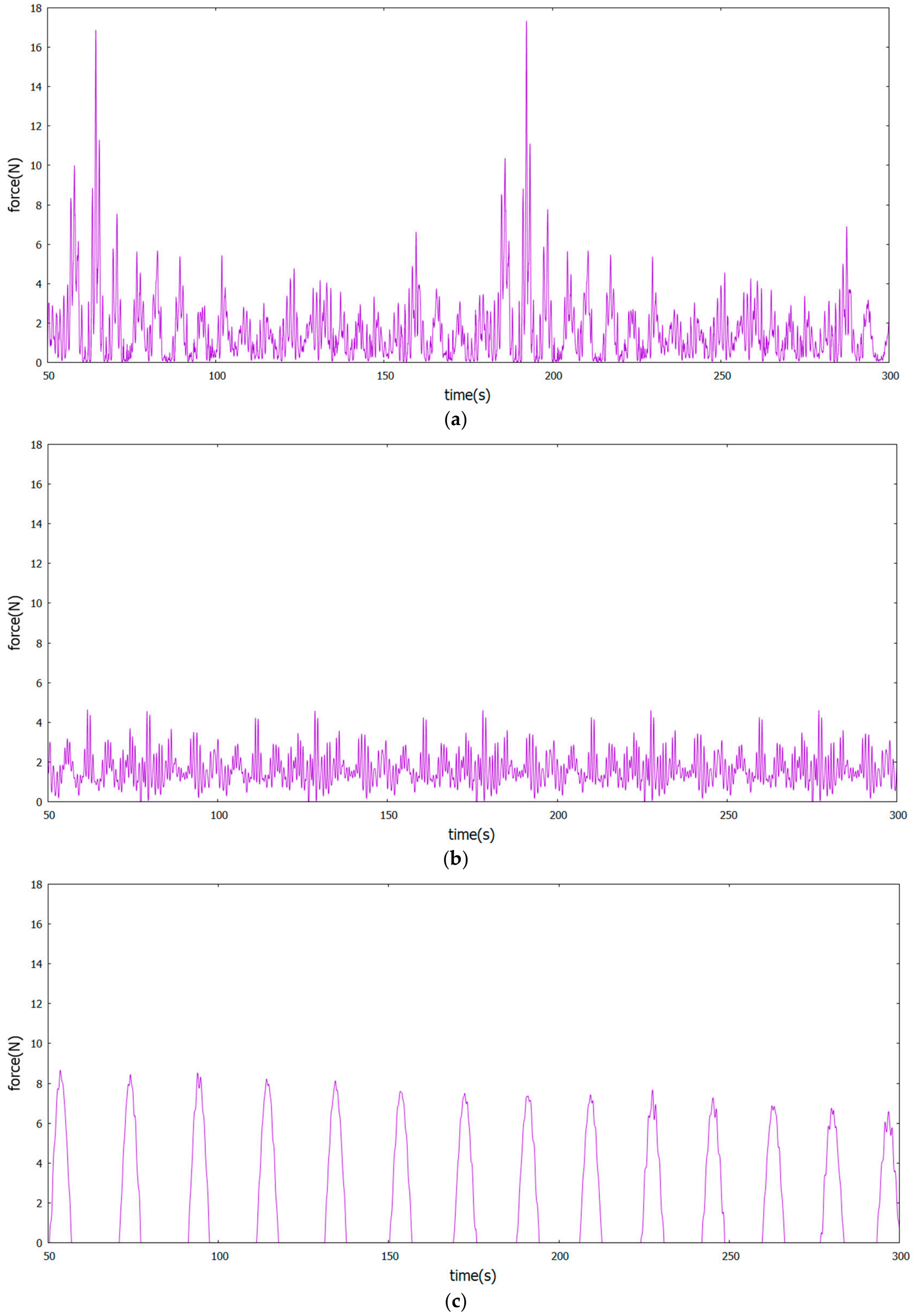

Figure 18. (**a**) Time series of mooring tension in experiments with buoy and inextensible cables (A) with T_p = 1 s for $H_s \approx 0.04$ m. (**b**) Time series of mooring tension from model with buoy and inextensible cables (A) with T_p =1 s for $H_s \approx 0.04$ m. (**c**) Time series of mooring tension from model with elastic cables to buoy and float (D) with T_p =1 s for $H_s \approx 0.04$ m.

The largest H_s was 0.13 m with T_p= 1.4 s. The experimental mooring force time series is shown in Figure 19a with a very large peak of about 140 N and a mean of about 50 N. A slowly varying drift force is evident. The model time series in Figure 19b has similar peak magnitudes but with a constant mean force imposed there is no slowly varying drift force. In the experiments, the drift force variation is not associated with groups of relatively large waves. With elastic cables to buoy and float in Figure 19c, the force has become almost constant and this is also the case with an inextensible cable (hawser) to the bow float. The cable does not become slack as the mean force is too large. This is generally the case for $H_s > 0.04$ m.

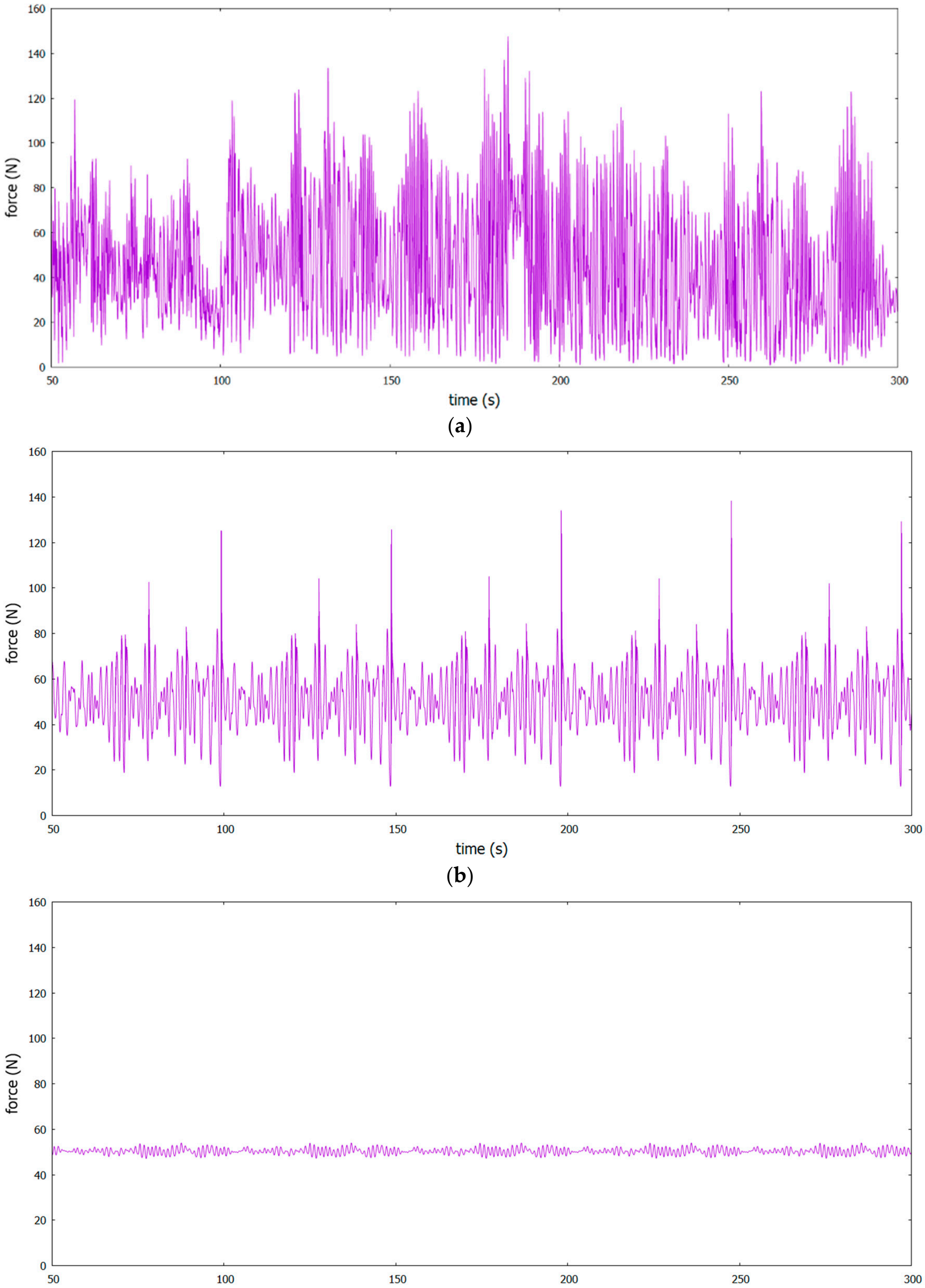

(**a**)

(**b**)

(**c**)

Figure 19. (**a**) Time series of mooring tension in experiments with buoy and inextensible cables (A) with T_p = 1.4 s for H_s = 0.13 m. (**b**) Time series of mooring tension from model with buoy and inextensible cables (A) with T_p = 1.4 s for H_s = 0.13 m. (**c**) Time series of mooring tension from model with elastic cables to buoy and float (D) with T_p =1.4 s for H_s = 0.13 m.

Some other mooring options may be tested. Pre-tension is sometimes used to reduce or avoid snap loads and a pre-tension of 3 N was tested with cables connected directly to the float base but the effect on results was minimal. The effect of a bigger buoy with diameter 0.15 m was also tested but again it had minimal effect. Adding clump masses, buoyant risers or both along mooring cables has been investigated in order to reduce snap loads [11,17,24], effectively increasing the hydrodynamic elasticity of the system, but this is not considered necessary here.

Most cases were also run with a cable elastic stiffness of 200 N/m. This did not change the underlying results; with elastic cables to buoy and to buoy and float, the snap loads in large waves were increased slightly over results with 100 N/m but were still only slightly greater than the mean forces. The cable extensions were roughly halved which may be a practical advantage.

The mean hydrodynamic force may be reduced by a current opposing the wave direction. For the case with T_p = 1.4 s and H_s = 0.13 m mean force was reduced by up to 90% but the snap load remained only slightly greater than the reduced mean force.

This analysis has been undertaken with a linear diffraction/radiation model with mean forces imposed. This is partially justified by the model predicting platform response quite accurately and the highly nonlinear mean force is from experimental measurement. There is qualitative prediction of snap loads with the inextensible cables used experimentally. For operational wave conditions there is some evidence that mean forces associated with groups of large waves may cause the model to underestimate local "mean" or drift force and correspondingly underestimate snap loads. This slowly varying drift force associated with intermittent groups should not be confused with low frequency forces due to difference frequency effects which have caused resonant response of offshore platforms. In this case, the resonant surge period is about 7 s. There is thus a limitation in assuming an overall mean for an irregular wave condition rather than a varying drift force. For very large waves slowly varying drift forces are observed but these do not now coincide with groups of larger waves; the waves are highly nonlinear, occasionally breaking, and dynamic interaction is clearly complex. Nevertheless, it is expected that the influence of elastic cables will also be predicted qualitatively, importantly reducing the snap loads to be just larger than the mean in large waves. However experimental verification is always desirable. The determination of mean force is clearly important. CFD is an option, e.g., [18,19], but very computationally demanding for design where many configurations and wave conditions need to be tested. Another option is to use nonlinear Froude-Krylov forcing with the other force components assumed to be linear. This was quite successful for a single buoy on an elastic cable [25] in steep non-breaking waves but underestimated snap loads in breaking waves. Such an approach may be tuned further and is efficient as only the nonlinear wave field without body interaction needs to be computed by CFD.

The mooring configurations applied here are idealized and define the force-displacement curves for the total system. These idealizations need to be converted to practical configurations, for example with several mooring lines to the buoy, like radial spokes. Effects of damping due to cable drag may be included and anchor loads determined. Damping is generally beneficial in reducing snap loads. Such design may be undertaken with commercial codes such as Orcaflex [26] or explored with open source codes such as MoorDyn [27]. The hydrodynamic force on the buoy is assumed to be only due to buoyancy relative to mean water level, ignoring the effect of drag, added mass and radiation. As the mooring forces are predicted reasonably in operational conditions this does not appear to be a major limitation. In extreme waves with elastic cables the buoy is fully submerged and the mooring force almost constant; drag and inertia are expected to be small in relation to buoyancy although this should be confirmed experimentally.

The focus of this study has been on snap loads. Fatigue is another important consideration which requires the running of many wave cases from a scatter diagram. Although snap loads for intermediate waves are much smaller than for large waves their impact on fatigue requires further study. There can relatively large snap loads measured experimentally in operational conditions associated with wave groups.

Full scale values may be determined based on Froude scaling. If a scale of 1:50 is assumed, appropriate for a site with predominant T_p of 8–9 s, the dry laboratory scale mass of 55.7 kg becomes nearly 7000 tons at full scale and the maximum snap load (close to the mean value) of about 55 N becomes 700 tons which is well within the breaking load limit for a polyester cable, as indicated in [15]. This extreme load is dependent on extreme wave statistics and will be greater for certain sites. In a practical mooring configuration load would be shared between several mooring lines, typically between 3 and 12 in a radial spoke arrangement.

5. Conclusions

The mooring forces on the 6-float wave energy converter M4 were measured in wave basin tests with inextensible cables attached to a mooring buoy and modelled in time-domain linear diffraction/radiation form with experimental mean forces input. Platform rotational response was well predicted and there was qualitative agreement of high snap loads in large waves. Elastic cables were then modelled in three idealized configurations: with direct connection to the base bow float, elastic connection to the buoy, and elastic connections to buoy and float. The quasi-static mooring models were almost exact. In large waves the snap loads with elastic cable to buoy were effectively avoided as they were only slightly greater than the mean force; the dynamic forces were thus very small. In operational waves the small snap loads measured experimentally could be underestimated due to wave group effects. The model thus requires input of the highly nonlinear mean hydrodynamic force which is known here from experiment but in general requires modelling, either from CFD or from partial CFD with nonlinear Froude-Krylov forcing. The idealized mooring configurations and modelling undertaken here provide basic information for detailed mooring analysis, including several cables, accounting for cable damping and buoy hydrodynamics with drag, inertia and added mass, as well as buoyancy. An important conclusion is that dynamic mooring loads are almost eliminated in large waves with an elastic cable to a buoy. That this applies for this particular M4 configuration does not mean it is a general rule and any configuration requires analysis.

Author Contributions: Conceptualization, methodology, modelling, experiments, writing, funding acquisition, P.S.; experiments, data analysis, project administration, E.C.M. All authors have read and agreed to the published version of the manuscript.

Funding: The experimental project M4WW was funded by the EU Marinet2 programme and ECM was supported at the University of Manchester by the Energy Sustainability Conacyt-SENER fund provided by the Mexican government.

Acknowledgments: Electronic instrumentation for the experimental program was provided Bob Brown.

Conflicts of Interest: The authors declare no conflict of interest.

References

1. Cruz, J. *Ocean Wave Energy*; Springer: New York, NY, USA, 2008.
2. Antonio, F.D.O. Wave energy utilization: A review of the technologies. *Renew. Sustain. Energy Rev.* **2010**, *14*, 899–918.
3. Stansby, P.; Moreno, E.C.; Stallard, T.; Maggi, A. Three-float broad-band resonant line absorber with surge for wave energy conversion. *Renew. Energy* **2015**, *78*, 132–140. [CrossRef]
4. Stansby, P.; Moreno, E.C.; Stallard, T. Large capacity multi-float configurations for the wave energy converter M4 using a time-domain linear diffraction model. *Appl. Ocean. Res.* **2017**, *68*, 53–64. [CrossRef]
5. Moreno, E.C.; Stansby, P. The 6-float wave energy converter M4: Ocean basin tests giving capture width, response and energy yield for several sites. *Renew. Sustain. Energy Rev.* **2019**, *104*, 307–318. [CrossRef]
6. Stansby, P.K.; Carpintero Moreno, E. Hydrodynamics of the multi-float wave energy converter M4 with slack moorings: Time domain linear diffraction-radiation modelling with mean force and experimental comparison. *Appl. Ocean. Res.* **2020**, *97*, 102070. [CrossRef]

7. Santo, H.; Taylor, P.H.; Moreno, E.C.; Stansby, P.; Taylor, R.E.; Sun, L.; Zang, J. Extreme motion and response statistics for survival of the three-float wave energy converter M4 in intermediate water depth. *J. Fluid Mech.* **2017**, *81*, 175–204. [CrossRef]
8. Lee, C.H.; Newman, J.N. *Wamit—User Manual Version 7.0*; WAMIT Inc.: Chestnut Hill, MA, USA, 2013.
9. DNV GL. *DNVGL-RP-C205 Environmental Conditions and Environmental Loads*; DNV GL: Oslo, Norway, 2017.
10. Johanning, L.; Smith, G.H. D7.3.2 Consideration of the Cost Implications for Mooring MEC Devices. EquiMar Protocols. 2009. Available online: http://www.equimar.org/equimar-project-deliverables.html (accessed on 10 October 2020).
11. Davidson, J.; Ringwood, J.V. Mathematical Modelling of Mooring Systems for Wave Energy Converters—A review. *Energies* **2017**, *10*, 666. [CrossRef]
12. Paduano, B.; Giorgi, G.; Gomes, R.P.F.; Pasta, E.; Henriques, J.C.C.; Gato, L.M.C.; Mattiazzo, G. Experimental Validation and Comparison of Numerical Models for the Mooring System of a Floating Wave Energy Converter. *J. Mar. Sci. Eng.* **2020**, *8*, 565. [CrossRef]
13. Thomsen, J.B.; Ferri, F.; Kofoed, J.P.; Black, K. Cost Optimization of Mooring Solutions for Large Floating Wave Energy Converters. *Energies* **2018**, *11*, 159. [CrossRef]
14. Amran, N.A.; Koto, J.; Sio, C.L. Review on Polyester Mooring Lines of Offshore Structures. *J. Ocean Mech. Aerosp. Sci. Eng.* **2016**, *35*, 7–12.
15. Harris, R.E.; Johanning, L.; Wolfram, J. Mooring systems for wave energy converters: A review of design issues and choices. *Proc. Inst. Mech. Eng. Part. B J. Eng. Manuf.* **2006**, *220*, 159–168.
16. Ridge, I.M.L.; Banfield, S.J.; Mackay, J. Nylon fibre rope moorings for wave energy converters. In Proceedings of the OCEANS 2010 MTS/IEEE SEATTLE, Seattle, WA, USA, 20–23 September 2010; pp. 1–10.
17. Weller, S.; Johanning, L.; Davies, P.; Banfield, S.J. Synthetic mooring ropes for marine renewable energy applications. *Renew. Energy* **2015**, *83*, 1268–1278. [CrossRef]
18. Palm, J.; Eskilsson, C.; Paredes, G.M.; Bergdahl, L. Coupled mooring analysis for floating wave energy converters using CFD: Formulation and validation. *Int. J. Mar. Energy* **2016**, *16*, 83–99. [CrossRef]
19. Sjokvist, L.; Wuc, J.; Ransley, E.; Engstrom, J.; Eriksson, M.; Goteman, M. Numerical models for the motion and forces of point-absorbing wave energy converters in extreme waves. *Ocean. Eng.* **2017**, *145*, 1–14. [CrossRef]
20. Giorgi, G.; Ringwood, J.V. Nonlinear Froude-Krylov and viscous drag representations for wave energy converters in the computation/fidelity continuum. *Ocean. Eng.* **2017**, *141*, 164–175. [CrossRef]
21. Giorgi, G.; Ringwood, J.V. Comparing nonlinear hydrodynamic forces in heaving point absorbers and oscillating wave surge converters. *J. Ocean. Eng. Mar. Energy.* **2018**, *4*, 25–35. [CrossRef]
22. Gu, H.; Stansby, P.; Stallard, T.; Carpintero Moreno, E. Drag, added mass and radiation damping of oscillating vertical cylindrical bodies in heave and surge in still water. *J. Fluids Struct.* **2018**, *82*, 343–356. [CrossRef]
23. Liao, Z.; Stansby, P.; Li, G. A generic linear non-causal optimal control framework integrated with wave excitation force prediction for multi-mode wave energy converters with application to M4. *Appl. Ocean. Res.* **2020**, *97*, 102056. [CrossRef]
24. Gao, Z.; Moan, T. Mooring system analysis of multiple wave energy converters in a farm configuration. In Proceedings of the 8th European Wave and Tidal Energy Conference, Uppsala, Sweden, 7–10 September 2009.
25. Lind, S.J.; Stansby, P.K.; Rogers, B.D. Fixed and moored bodies in steep and breaking waves using SPH with the Froude Krylov approximation. *J. Ocean Eng. Mar. Energy* **2016**, *2*, 331–354. [CrossRef]
26. Orcaflex. 2020. Available online: www.orcina.com/orcaflex (accessed on 10 October 2020).
27. Hall, M.; Goupee, A. Validation of a lumped-mass mooring line model with DeepCwind semi-submersible model test data. *Ocean. Eng.* **2015**, *104*, 590–603. [CrossRef]